

Facoltà di Scienze e Tecnologie Laurea Triennale in Fisica

Thermal effects on phonon friction in a channeling model

Advisor: Prof. Nicola Manini

Nicolas Gialnisio Matricola n° 990042 A.A. 2024/2025

Thermal effects on phonon friction in a channeling model

Nicolas Gialnisio Dipartimento di Fisica, Università degli Studi di Milano, Via Celoria 16, 20133 Milano, Italia

October 29, 2025

Abstract

In this thesis we study the temperature dependence of phonon friction acting on a particle sliding through a simple cubic crystal, by extending and evaluating an expression derived in a previous work. We focus on the Debye-Waller factor, which carries all the temperature dependence of the phonon friction. The main results reported here are: (i) the full isotropy of the **Q**-dependence of the Debye-Waller factor for the simple-cubic crystal; (ii) a factorization allowing us to predict the entire velocity and temperature dependence of friction at the cost of its evaluation at one single temperature, to a very good degree of approximation.

Advisor: Prof. Nicola Manini

Contents

1	Introduction			
2	The	e model	3	
	2.1	The Debye-Waller exponent	5	
3	The	eory	8	
	3.1	Symmetry of the Debye–Waller exponent	8	
		3.1.1 Symmetries of the crystal	10	
		3.1.2 Simplifying the quadratic terms	12	
		3.1.3 Summing the k on diagonal	14	
		3.1.4 Canceling cross products out	16	
	3.2	A Debye-like approximation	17	
	3.3	Useful symmetries for the evaluation of $C(T)$	18	
	3.4	Size scaling for the $C(T)$ coefficient	19	
4	Res	sults	22	
5	Discussion and Conclusion 2			
\mathbf{A}	A A few basic crystal symmetries			
В	3 Symmetry for faster $C(T)$ computation			
$\mathbf{R}_{f \epsilon}$	efere	ences	32	

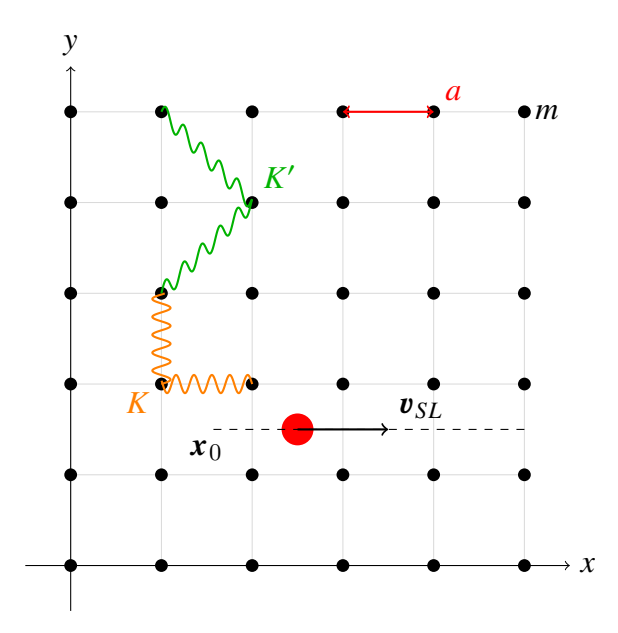


Figure 1: A sketch of the particle-crystal model viewed down the \hat{z} axis. The simple-cubic crystal consists of $N=N_{\rm side}^3$ particles (black dots) of mass m connected by springs with elastic constants K (nearest neighbors) and K' (second/face-diagonal neighbors). We assume $K'=\frac{1}{2}K$. a is the equilibrium lattice spacing. Red dot: the sliding particle, characterized by a very large mass M; x_0 is its initial position.

1 Introduction

Friction is intimately connected to the dissipation of ordered kinetic energy into vibrational waves of the objects in mutual contact. When these objects are crystalline solids, this amounts to the excitation of phonons. Recently a novel method for evaluating this friction has been proposed [1]. This method, rather than on traditional molecular dynamics (MD) simulations, relies on an analytical formula derived using linear response theory in a simplified geometry (channeling). So far, this method has been applied to crystals kept at zero temperature. In this work, we will investigate the temperature dependence of friction, through an extension of the same analytic method.

2 The model

The model, Figure 1, consists in a simple cubic crystal across which a particle ("the slider") moves. We assume that the slider moves along a crystal high

Physical quantity	Symbol	Typical value
Length	а	$500\mathrm{pm}$
Mass	m	$5 \times 10^{-26} \text{ kg}$
Spring constant	K	$300 \: \rm N \: m^{-1}$
Time	$(m/K)^{1/2}$	$1.3 \times 10^{-14} \text{ s}$
Frequency	$(K/m)^{1/2}$	$7.7 \times 10^{13} \text{ s}^{-1}$
Velocity	$a(K/m)^{1/2}$	$3.9 \times 10^4 \text{ m/s}$
Force	Ka	$1.5 \times 10^{-7} \text{ N}$
Energy	Ka^2	$7.5 \times 10^{-17} \text{ J}$
Temperature	Ka^2/k_B	$5.4 \times 10^6 \text{ K}$
Debye Temperature	$ heta_D$	$1958~\mathrm{K}$
Action	$a^2(Km)^{1/2}$	$9.7 \times 10^{-31} \text{ Js}$

Table 1: Physical quantities in the adopted model, with mathematical symbols, expressions, and their typical values.

symmetry direction, for example the x axis, with velocity $\mathbf{v}_{SL} = v_{SL} \mathbf{e}_x$. We also postulate that it starts off at a symmetric position inside the crystalline channel, i.e. exactly midway between lines of atoms. The kinetic energy of the slider decreases due to a sequence of collisions with the crystal, where it is assumed to generate only phononic excitations. More specifically, see Table 1, the model proposes a simple cubic crystal characterized by particles of mass m connected by harmonic nearest and second-neighbor springs with elastic constants K and K' and equilibrium lengths a and $\sqrt{2a}$, respectively, which guarantee the mechanical stability and determine the phonon dispersions.

The previous work [1] derived the following analytical expression for the average friction force which slows the slider down:

$$F_{T}(v_{SL}) = \frac{\pi}{2ma^{3}} \sum_{\mathbf{G}_{\perp}} e^{-i\mathbf{x}_{0} \cdot \mathbf{G}_{\perp}} \int_{\Omega} \frac{d^{3}\mathbf{Q}}{(2\pi^{3})} Q_{x} \tilde{V}(|\mathbf{Q}|) \tilde{V}(|\mathbf{Q} + \mathbf{G}_{\perp}|) e^{-W(\mathbf{Q})} e^{-W(\mathbf{Q} + \mathbf{G}_{\perp})} \times$$

$$\times \sum_{\lambda=1}^{3} \mathbf{Q} \cdot \boldsymbol{\epsilon}_{\lambda}(\mathbf{Q}) (\mathbf{Q} + \mathbf{G}) \cdot \boldsymbol{\epsilon}_{\lambda}(\mathbf{Q}) \mathcal{L}(\mathbf{Q}, v_{SL}, \gamma) ,$$
with
$$\mathcal{L}(\mathbf{Q}, v_{SL}, \gamma) = \frac{\gamma}{2\pi} \frac{4Q_{x}v_{SL}}{[(Q_{x}v_{SL} - \omega_{\lambda}(\mathbf{Q}))^{2} + (\frac{\gamma}{2})^{2}][(Q_{x}v_{SL} + \omega_{\lambda}(\mathbf{Q}))^{2} + (\frac{\gamma}{2})^{2}]},$$

$$(1)$$

where:

- \circ *T* is the temperature;
- $\circ x_0$ is the initial position of the slider;

- G_{\perp} are the reciprocal lattice vectors perpendicular to the direction \hat{x} of the slider velocity;
- $\circ \tilde{V}(|Q|)$ is the Fourier transform of the slider-crystal-atom interaction V(r), which can be any function whose Fourier Transform exists.
- $\circ e^{-W(\mathbf{Q})}$ is the Debye-Waller factor, defined below, which was approximated to unity in the numerical calculations carried out in the previous work [1];
- $\circ \gamma$ is the phonon damping rate;
- \circ Ω is the **Q**-integration domain, namely the octant with all positive components.

In the present thesis, we restore the Debye-Waller factors, without approximating them with unity, and we study their effects on friction. Since all the temperature dependence of friction in Eq. (1) lies precisely inside the Debye-Waller factors, their study is equivalent to an investigation of the explicit temperature dependence of friction.

2.1 The Debye-Waller exponent

In Ref. [1], the following expression for the Debye-Waller factor exponent is derived:

$$W(\mathbf{Q}) = \frac{1}{2N} \sum_{k=1}^{1BZ\setminus\{0\}} \sum_{\lambda=1}^{3} |\mathbf{Q} \cdot \boldsymbol{\epsilon}_{\lambda}(\mathbf{k})|^{2} \frac{\hbar}{2m\omega_{\lambda}(\mathbf{k})} (2n_{\lambda}(\mathbf{k}) + 1), \qquad (2)$$

where:

- \circ Q is a point in reciprocal space;
- N is the number of atoms within the cubic crystal volume $N a^3 = (N_{\text{side}} a)^3$ (to which periodic boundary conditions are applied), or equivalently the number of k points within the first Brillouin zone;
- $1BZ \setminus \{0\}$ stands for the sampling grid of the first Brillouin zone, without the origin (see further below);
- λ is an index spanning the three phonon polarization branches of the cubic crystal;
- \circ $\epsilon_{\lambda}(k)$ is the polarization vector for the λ branch evaluated at the k point;
- $\circ \ \omega_{\lambda}(\mathbf{k})$ is the corresponding angular frequency;

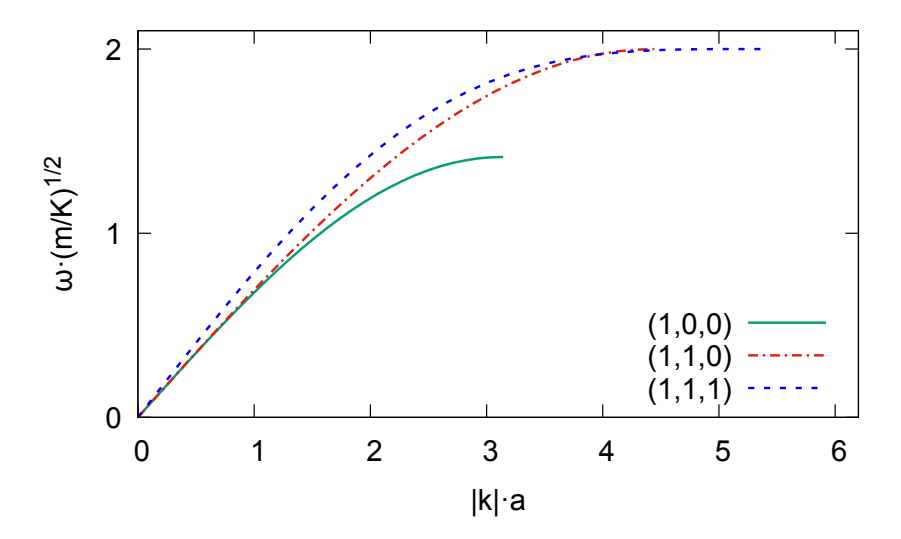


Figure 2: Phonon dispersion of the lowest transverse branch $(\lambda = 1)$ of the simple-cubic crystal, along three different directions in reciprocal space. Note the acoustic behavior (frequency vanishing linearly for $|\mathbf{k}| \to 0$), with different slopes (speeds of sound) depending on the \mathbf{k} -space direction.

• $n_{\lambda}(\mathbf{k})$ is the average equilibrium number of quanta (phonons) of the λ , \mathbf{k} oscillator at temperature T.

In Equation (2) the phonon frequency $\omega_{\lambda}(\mathbf{k})$ is at the denominator. As a result, any term with vanishing frequency diverges. In practice only the 3 $\mathbf{k} = \mathbf{0}$ modes have vanishing frequency, and therefore they are omitted from the summation. However, the small- \mathbf{k} terms have a very small denominator, leading to them dominating the Debye Waller exponent. This issue will make it rather the sampling of the small- \mathbf{k} region rather delicate.

The number of phonons $n_{\lambda}(\mathbf{k})$ carries all the temperature dependence of Eq. (2), and it is evaluated according to Bose-Einstein statistics (3):

$$n_{\lambda}(\mathbf{k}) = \frac{1}{\exp\left(\frac{\hbar \,\omega_{\lambda}(\mathbf{k})}{k_{B}T}\right) - 1} \,. \tag{3}$$

Now, consider the phonon occupation factor, Equation (2), in the limit $T \to 0$, Fig. 3:

$$\lim_{T \to 0} \frac{1}{\exp\left(\frac{\hbar \,\omega_{\lambda}(\mathbf{k})}{k_B T}\right) - 1} = 0. \tag{4}$$

The number of phonons vanishes exponentially rapidly for $T\to 0$ and, as a result, the phonon factor $(2n_{\lambda}(k)+1)\to 1$ in C(T) goes to unity, as temperature

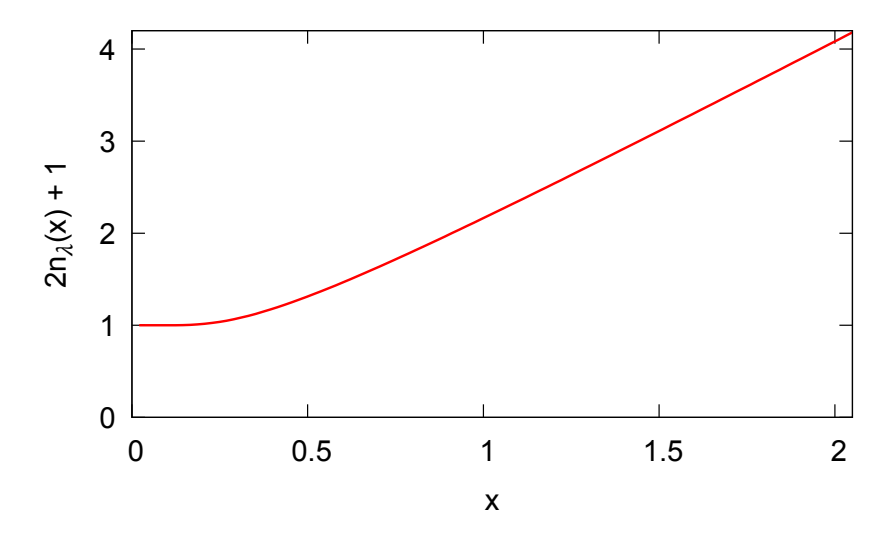


Figure 3: The generic trend of the phonon occupation factor as a function of $x = (k_B T)/(\hbar \omega)$.

decreases to zero, indicating that atoms oscillate even at T=0. This zero-point effect makes W(T) nonzero and thus the Debye-Waller different from unity even at T=0. Clearly this small effect was entirely neglected when the Debye-Waller factor was approximated to unity [1].

At high temperature $T \gg \hbar \omega_{\lambda}(T)/k_B$, the phonon occupation factor becomes approximately linearly dependent on T, reflecting the classical limit of Bose–Einstein statistics:

$$2n_{\lambda}(\mathbf{k}) + 1 \simeq \frac{2k_B}{\hbar\omega_{\lambda}(\mathbf{k})}T \quad \text{for } T \to +\infty,$$
 (5)

At high temperatures, the thermal energy k_BT is much larger than the spacing between the quantized energy levels of the harmonic oscillator. As a result, these levels can be regarded as quasi-continuous, and the oscillator crosses over from quantum to classical behavior. If the phonon occupation number becomes $n_{\lambda}(\mathbf{k}) \simeq k_B T/(\hbar \omega_{\lambda}(\mathbf{k}))$, then the energy of that harmonic oscillator becomes $\simeq k_B T$, which coincides with result of the energy equipartition theorem. Finally, we recognize the entire product $\frac{\hbar}{2m\omega_{\lambda}(\mathbf{k})}(2n_{\lambda}(\mathbf{k})+1)$ in Eq. (2) as the mean square oscillatory amplitude of a one-dimensional harmonic oscillator in the $n_{\lambda}(\mathbf{k})$ -th excited state. To sum up, Equation (2) shows a sum of the mean amplitudes of oscillators for each polarization weighted by the projection between the wavevector \mathbf{Q} and all the directions of oscillation.

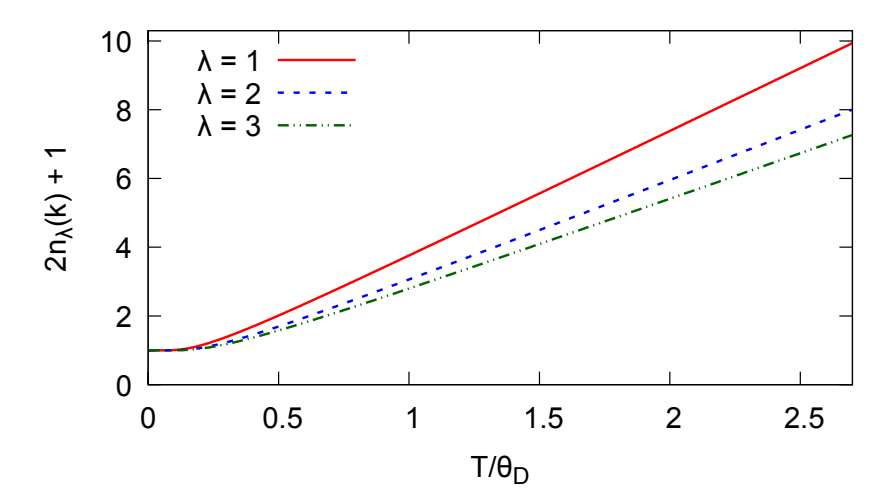


Figure 4: Phonon occupation factors for the simple-cubic crystal with the dynamical parameters defined in Table 1, as a function of temperature, evaluated at the $\mathbf{k} = (1, 2, 3) \frac{1}{a}$ point, where the three phonon frequencies $\omega_1(\mathbf{k}) = 1.80 \ (K/m)^{1/2}$, $\omega_2(\mathbf{k}) = 2.24 \ (K/m)^{1/2} \ \omega_3(\mathbf{k}) = 2.48 \ (K/m)^{1/2}$. The nonzero intercept is the same, while the high-temperature approximately linear increase occurs with different slopes, each inversely proportional to its mode frequency.

3 Theory

3.1 Symmetry of the Debye–Waller exponent

In the present section we investigate the symmetry properties of W(Q). As shown in Fig. 5, the numerical evaluation of W(Q) shows that its value only depends on |Q|, indicating full rotational symmetry. Figure 5 also shows an exactly quadratic dependence on |Q|.

However, at face value this rotational symmetry and quadratic dependence are far from obvious. They require an analytical proof. The goal of the following calculations is to factorize W(Q) into two terms: $W(Q) = |Q|^2 \cdot C(T)$. In this way we evaluate C(T) for any T and afterwards we bring its value inside the numerical computation of the friction, at no extra computational cost within the integration of Eq. (1). Without these symmetries, it would be necessary to repeatedly evaluate the entire W(Q) for every Q in the grid over which the integral of Eq. (1) is computed.

The key is to split the entire summation into sets and derive the symmetry

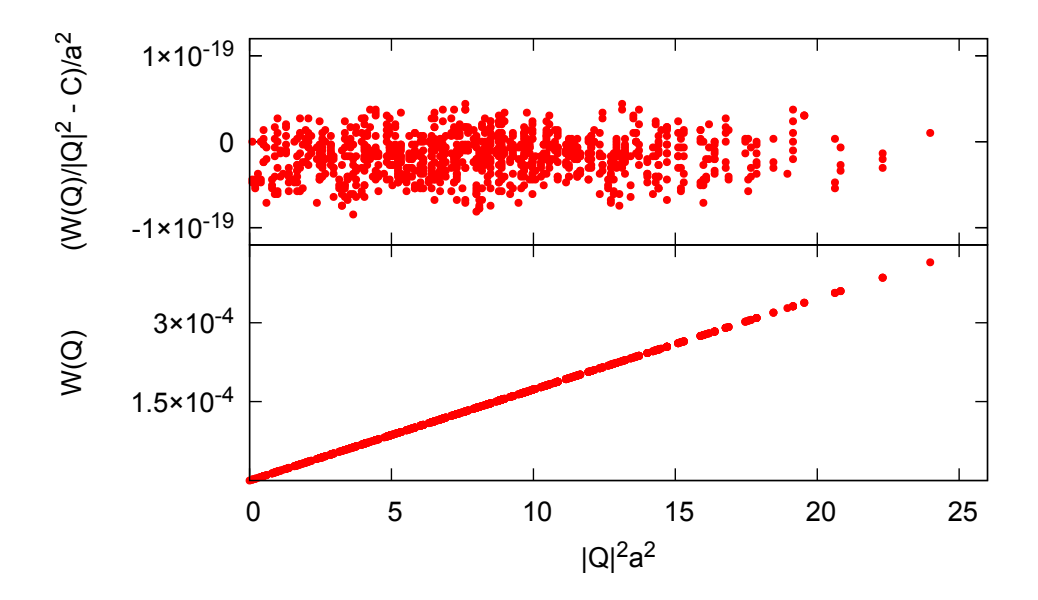


Figure 5: Debye–Waller exponent evaluated at the temperature $T = 0.16 \,\theta_D$, as a function of $|\mathbf{Q}|^2$ at, computed on a cubic mesh of 1000 k-points within the first Brillouin zone. The resulting prefactor $C(T) \simeq 1.73 \times 10^{-5} \, a^2$. The upper panel highlights the negligibly tiny deviations of the numerical determination from this value, further confirming the \mathbf{Q} -isotropy of $W(\mathbf{Q})$.

from each of these. First of all, it is useful to simplify the notation:

$$W(\mathbf{Q}) = \frac{1}{2N} \sum_{\mathbf{k}}^{1BZ\setminus\{\mathbf{0}\}} \sum_{\lambda=1}^{3} |\mathbf{Q} \cdot \boldsymbol{\epsilon}_{\lambda}(\mathbf{k})|^{2} Y_{\lambda}(\mathbf{k}), \qquad (6)$$

$$Y^{\lambda}(\mathbf{k},T) = \frac{\hbar}{2m\omega_{\lambda}(\mathbf{k})} (2n_{\lambda}(\mathbf{k},T) + 1).$$
 (7)

Another change in notation, useful for clearness, is to move the subscript up like this $\epsilon_{\lambda}(\mathbf{k}) \to \epsilon^{\lambda}(\mathbf{k})$ to gain space for the component index $\epsilon_{i}^{\lambda}(\mathbf{k})$; from now on, the two notations will be equivalent.

To start, consider a single k within the first Brillouin zone, compute the

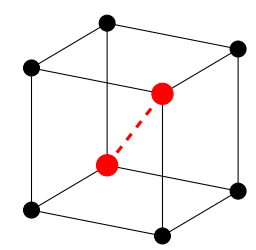


Figure 6: Simple cubic lattice, with one of the main diagonals highlighted, for example (1, 1, 1).

square and the sum on λ like in Equation (8),

$$\sum_{\lambda} (Q_{x} \epsilon_{x}^{\lambda} + Q_{y} \epsilon_{y}^{\lambda} + Q_{z} \epsilon_{z}^{\lambda})^{2} Y^{\lambda} =$$

$$= Q_{x}^{2} (\epsilon_{x}^{1^{2}} Y^{1} + \epsilon_{x}^{2^{2}} Y^{2} + \epsilon_{x}^{3^{2}} Y^{3}) +$$

$$+ Q_{y}^{2} (\epsilon_{y}^{1^{2}} Y^{1} + \epsilon_{y}^{2^{2}} Y^{2} + \epsilon_{y}^{3^{2}} Y^{3}) +$$

$$+ Q_{z}^{2} (\epsilon_{z}^{1^{2}} Y^{1} + \epsilon_{z}^{2^{2}} Y^{2} + \epsilon_{z}^{3^{2}} Y^{3}) +$$

$$+ Q_{z}^{2} (\epsilon_{z}^{1^{2}} Y^{1} + \epsilon_{z}^{2^{2}} Y^{2} + \epsilon_{z}^{3^{2}} Y^{3}) +$$

$$+ 2Q_{x} Q_{y} (\epsilon_{x}^{1} \epsilon_{y}^{1} Y^{1} + \epsilon_{x}^{2} \epsilon_{y}^{2} Y^{2} + \epsilon_{x}^{3} \epsilon_{y}^{3} Y^{3}) +$$

$$+ 2Q_{y} Q_{z} (\epsilon_{y}^{1} \epsilon_{z}^{1} Y^{1} + \epsilon_{y}^{2} \epsilon_{z}^{2} Y^{2} + \epsilon_{y}^{3} \epsilon_{z}^{3} Y^{3}) .$$

$$(8)$$

The first three lines after the equal sign are quadratic in the components and the last three have mixed terms. With the aim of the proof in mind it we look for a way to make the brackets that multiply the quadratic term equal and to make those multiplying the mixed ones vanish; in this way, the brackets can be factored out and multiplied by the squared norm of \mathbf{Q} , obtaining $C(T) \cdot |\mathbf{Q}|^2$. The idea is to sum other addends to this above, to cancel out or factorize the terms. Focusing on the first three rows, it makes sense to look for other two addends in such a way that Y^{λ} keeps the same value and the sum of $\epsilon_i^{\lambda^2}$ is equal to one, like the norm of the polarization vector $\boldsymbol{\epsilon}$. Now, it is useful to analyze the symmetries of the crystal to deduce some simplifications.

3.1.1 Symmetries of the crystal

The crystal lattice considered has a simple-cubic structure and so the reciprocal lattice, see Figure 6. Permuting the components of the position vector \mathbf{x} of each atom in the same way, one obtains the same crystal; so, rotations around on of the main diagonal, see Figure 6, and reflections, with respect to the three planes passing through the main diagonal and one of the three axis x,y,z, are all symmetries. These symmetries are induced even on the reciprocal lattice.

Consider a set of three k, obtained by permuting their components so that no components remain in the same position, or in other words, obtained by rotating one of them around the reciprocal lattice main diagonal, (1, 1, 1) in Miller indexes, by 120° , namely,

$$\mathbf{k}_{1} = (k_{1}, k_{2}, k_{3})$$

$$\mathbf{k}_{2} = (k_{2}, k_{3}, k_{1})$$

$$\mathbf{k}_{3} = (k_{3}, k_{1}, k_{2}),$$
(9)

it is possible to use the symmetry of the lattice, Appendix 5, to assert

$$Y^{\lambda}(\boldsymbol{k}_1) = Y^{\lambda}(\boldsymbol{k}_2) = Y^{\lambda}(\boldsymbol{k}_3), \qquad (10)$$

and

$$\boldsymbol{\epsilon}^{\lambda}(\boldsymbol{k}_{1}) = (\epsilon_{1}, \epsilon_{2}, \epsilon_{3})$$

$$\boldsymbol{\epsilon}^{\lambda}(\boldsymbol{k}_{2}) = \pm(\epsilon_{2}, \epsilon_{3}, \epsilon_{1})$$

$$\boldsymbol{\epsilon}^{\lambda}(\boldsymbol{k}_{3}) = \pm(\epsilon_{3}, \epsilon_{1}, \epsilon_{2}).$$
(11)

Equation (10) is justified by the fact that all the k dependence is within the frequency $\omega^{\lambda}(k)$, which is not a vector, meaning that does not rotate with the crystal if one applies the rotational symmetry, so it sees these three points like they were the same, due to their symmetry equivalence. Similarly, in (11) the components of the polarization vectors remain the same after the rotation, but in this case the vector rotates with the lattice, and, since the rotation is the same around the (1,1,1) diagonal, the effect is the same permutation of components. Actually, each polarization vector is obtained as an eigenvector of the dynamical matrix and, like any eigenvector, is defined only up to an overall sign. Consequently, although the effect of the rotation is merely a permutation, solving the eigenvalue problem for the rotated dynamical matrix may yield the same polarization vector but with the opposite global sign.

This argument seems to be inconsistent if one considers the points on the (1,1,1) diagonal, because it is impossible to obtain permuted polarization vectors starting from exactly the same k vector. In fact, polarization vectors are obtained as eigenvectors of the dynamical matrix evaluated for a specific k, therefore, the same matrix cannot have different eigenvectors. But in the case of a dynamical matrix evaluated on a k on the (1,1,1) diagonal, the three eigenvectors have the following proprieties:

1. one of the eigenvectors lies on the same direction of k, like always actually, but in this case also on the main diagonal, which means that remains the same after an arbitrary rotation around that axis;

2. the two eigenvectors, which are not lying on the main diagonal, have the same eigenvalue, therefore, they are defined up to a phase, and one can rotate them by hand after the rotation of the lattice.

This shows that that the arguments is valid also for those k vectors.

3.1.2 Simplifying the quadratic terms

For now, all k vectors lying on the main diagonal are ignored. Consider the sum over the set consisting of the three, aforementioned in (9), k vectors and extract from those the terms which are carrying the quadratic x-component of the Q vector. It is always possible to divide by three the total number of points N inside the cubic first Brillouin zone, $N = N_{\rm side}^3$, where $N_{\rm side}$ is the number of k on a side of the cube, minus the ignored ones in the main diagonal, which are $N_{\rm side}$. In fact, $N_{\rm side}^3 - N_{\rm side}$ is a multiple of three for every $N_{\rm side} \geq 2$ as $N_{\rm side}^3 - N_{\rm side} = N_{\rm side}(N_{\rm side}^2 - 1) = (N_{\rm side} - 1)N_{\rm side}(N_{\rm side} + 1)$, and one of the three must be a multiple of three. The argument is also valid for the remaining components.

$$\sum_{\boldsymbol{k}=\boldsymbol{k}_{1},\boldsymbol{k}_{2},\boldsymbol{k}_{3}} \sum_{\lambda} (Q_{x} \epsilon_{x}^{\lambda}(\boldsymbol{k}) + Q_{y} \epsilon_{y}^{\lambda}(\boldsymbol{k}) + Q_{z} \epsilon_{z}^{\lambda}(\boldsymbol{k}))^{2} Y^{\lambda}(\boldsymbol{k})$$

$$\rightarrow \sum_{\boldsymbol{k}=\boldsymbol{k}_{1},\boldsymbol{k}_{2},\boldsymbol{k}_{3}} Q_{x}^{2} (\epsilon(\boldsymbol{k})_{x}^{1^{2}} Y(\boldsymbol{k})^{1} + \epsilon(\boldsymbol{k})_{x}^{2^{2}} Y(\boldsymbol{k})^{2} + \epsilon(\boldsymbol{k})_{x}^{3^{2}} Y(\boldsymbol{k})^{3})$$

$$(12)$$

$$\begin{pmatrix} \epsilon_{x}^{\lambda}(\mathbf{k}_{1}) & \epsilon_{x}^{\lambda}(\mathbf{k}_{2}) & \epsilon_{x}^{\lambda}(\mathbf{k}_{3}) \\ \epsilon_{y}^{\lambda}(\mathbf{k}_{1}) & \epsilon_{y}^{\lambda}(\mathbf{k}_{2}) & \epsilon_{y}^{\lambda}(\mathbf{k}_{3}) \\ \epsilon_{z}^{\lambda}(\mathbf{k}_{1}) & \epsilon_{z}^{\lambda}(\mathbf{k}_{2}) & \epsilon_{z}^{\lambda}(\mathbf{k}_{3}) \end{pmatrix} = \begin{pmatrix} \epsilon_{1}^{\lambda} & \epsilon_{2}^{\lambda} & \epsilon_{3}^{\lambda} \\ \epsilon_{1}^{\lambda} & \epsilon_{2}^{\lambda} & \epsilon_{3}^{\lambda} & \epsilon_{1}^{\lambda} \\ \epsilon_{3}^{\lambda} & \epsilon_{1}^{\lambda} & \epsilon_{2}^{\lambda} \end{pmatrix}. \tag{13}$$

In Equation (13) the three polarization vectors are arranged into a matrix, in which the sign of the components are ignored, yielding a 3×3 matrix, whose columns are normalized to 1. By substituting the values of each components, using Equation (11), the rows also consist of vectors normalized to 1, because the matrix is symmetric. This is true even considering the correct sign of each component. This allows us to factorize the brackets multiplied by $Y^{\lambda}(\mathbf{k})$, which we recognize as the norm of the polarization vector, and we write the expression

in Equation (12) in this way:

$$\sum_{\mathbf{k}=\mathbf{k}_{1},\mathbf{k}_{2},\mathbf{k}_{3}} Q_{x}^{2}(\epsilon(\mathbf{k})_{x}^{12}Y(\mathbf{k})^{1} + \epsilon(\mathbf{k})_{x}^{22}Y(\mathbf{k})^{2} + \epsilon(\mathbf{k})_{x}^{32}Y(\mathbf{k})^{3}) =$$

$$= Q_{x}^{2} [(\epsilon_{x}^{1}(\mathbf{k}_{1})^{2} + \epsilon_{x}^{1}(\mathbf{k}_{2})^{2} + \epsilon_{x}^{1}(\mathbf{k}_{3})^{2})Y^{1} +$$

$$+ (\epsilon_{x}^{2}(\mathbf{k}_{1})^{2} + \epsilon_{x}^{2}(\mathbf{k}_{2})^{2} + \epsilon_{x}^{2}(\mathbf{k}_{3})^{2})Y^{2} +$$

$$+ (\epsilon_{x}^{3}(\mathbf{k}_{1})^{2} + \epsilon_{x}^{3}(\mathbf{k}_{2})^{2} + \epsilon_{x}^{3}(\mathbf{k}_{3})^{2})Y^{3}] =$$

$$= Q_{x}^{2} [(\epsilon_{1}^{12} + \epsilon_{2}^{12} + \epsilon_{x}^{12})Y^{1} +$$

$$+ (\epsilon_{2}^{22} + \epsilon_{3}^{22} + \epsilon_{1}^{22})Y^{2} +$$

$$+ (\epsilon_{3}^{32} + \epsilon_{1}^{32} + \epsilon_{2}^{32})Y^{3}] =$$

$$= Q_{x}^{2} (Y^{1} + Y^{2} + Y^{3}).$$
(14)

Replacing the index x by y or z leaves the argument unchanged. Therefore, the first three lines of Equation (8), after a summation on the vectors shown in Equation (9), we obtain Equation (15).

$$Q_{x}^{2}(Y^{1} + Y^{2} + Y^{3}) + Q_{y}^{2}(Y^{1} + Y^{2} + Y^{3}) + Q_{z}^{2}(Y^{1} + Y^{2} + Y^{3}) =$$

$$= |Q|^{2}(Y^{1} + Y^{2} + Y^{3}) =$$

$$= |Q|^{2} \sum_{\lambda} Y(\mathbf{k})^{\lambda} = \frac{1}{3} |Q|^{2} \sum_{\mathbf{k} = \mathbf{k}_{1}, \mathbf{k}_{2}, \mathbf{k}_{3}} \sum_{\lambda} Y(\mathbf{k})^{\lambda}.$$
(15)

The last step is carried out by considering Equation (10), and it is useful for coding purposes and for the approximation in Section 3.2. Now, sum over all the sets of three rotated k it is possible to make, which are a number M equal to $\frac{N_{\text{side}}^3 - N_{\text{side}}}{3}$. These sets are disjoint, we can label them using an index, and we can recover entirety of the first Brillouin zone, excluding the diagonal, by summing over that index, namely,

$$\sum_{j=1}^{M} \frac{1}{3} |\mathbf{Q}|^{2} \sum_{\mathbf{k}^{j} = \mathbf{k}_{1}^{j}, \mathbf{k}_{2}^{j}, \mathbf{k}_{3}^{j}} \sum_{\lambda} Y(\mathbf{k})^{\lambda} = \frac{1}{3} |\mathbf{Q}|^{2} \sum_{j=1}^{M} \sum_{\mathbf{k}^{j} = \mathbf{k}_{1}^{j}, \mathbf{k}_{2}^{j}, \mathbf{k}_{3}^{j}} \sum_{\lambda} Y(\mathbf{k})^{\lambda} = \frac{1}{3} |\mathbf{Q}|^{2} \sum_{\mathbf{k}^{j} = \mathbf{k}_{1}^{j}, \mathbf{k}_{2}^{j}, \mathbf{k}_{3}^{j}} \sum_{\lambda} Y(\mathbf{k})^{\lambda} = \frac{1}{3} |\mathbf{Q}|^{2} \cdot C'(T),$$
(16)

where $\{(k, k, k)\}$ stands for all the points on the main diagonal (1, 1, 1). This is similar to the final form for $W(\mathbf{Q})$, since all temperature dependence is collected in a separate term C'(T) that is multiplied by the squared norm of \mathbf{Q} . However, some steps are still missing. First of all, the terms on the diagonal still need to be summed, and then it remains to show how the cross terms cancel out.

3.1.3 Summing the k on diagonal

The statement we need to add the diagonal elements is the following:

$$\sum_{\lambda} |\boldsymbol{Q} \cdot \boldsymbol{\epsilon}_{\lambda}(\boldsymbol{k})|^{2} Y_{\lambda}(\boldsymbol{k}) = \frac{1}{3} |\boldsymbol{Q}|^{2} \sum_{\lambda} Y_{\lambda}(\boldsymbol{k}), \qquad (17)$$

which can be derived by summing three times over the same k, which can be seen as the permutation of itself:

$$3\sum_{\lambda} |\boldsymbol{Q} \cdot \boldsymbol{\epsilon}_{\lambda}(\boldsymbol{k})|^{2} Y_{\lambda}(\boldsymbol{k}) = \frac{1}{3} |\boldsymbol{Q}|^{2} \sum_{\boldsymbol{k}=\boldsymbol{k}_{1},\boldsymbol{k}_{2},\boldsymbol{k}_{3}} \sum_{\lambda} Y_{\lambda}(\boldsymbol{k}) = \frac{1}{3} |\boldsymbol{Q}|^{2} \cdot 3 \sum_{\lambda} Y_{\lambda}(\boldsymbol{k})$$

$$\Rightarrow \sum_{\lambda} |\boldsymbol{Q} \cdot \boldsymbol{\epsilon}_{\lambda}(\boldsymbol{k})|^{2} Y_{\lambda}(\boldsymbol{k}) = \frac{1}{3} |\boldsymbol{Q}|^{2} \sum_{\lambda} Y_{\lambda}(\boldsymbol{k}) = \frac{1}{3} |\boldsymbol{Q}|^{2} (2Y + Y^{3}),$$
(18)

where $Y^1 = Y^2 = Y$, $k_1 = k_2 = k_3$ and conditions in Equation (10) and (11) have been used. In this case, Equation (10) is true, because k is always the same. However, Equation (11) seems to be problematic, because one cannot now consider ϵ as permuted. Consider again Equation (14), in this case becomes:

$$Q_{x}^{2}[(\epsilon_{x}^{1}(\mathbf{k}_{1})^{2} + \epsilon_{x}^{1}(\mathbf{k}_{2})^{2} + \epsilon_{x}^{1}(\mathbf{k}_{3})^{2})Y^{1} + (\epsilon_{x}^{2}(\mathbf{k}_{1})^{2} + \epsilon_{x}^{2}(\mathbf{k}_{2})^{2} + \epsilon_{x}^{2}(\mathbf{k}_{3})^{2})Y^{2} + (\epsilon_{x}^{3}(\mathbf{k}_{1})^{2} + \epsilon_{x}^{3}(\mathbf{k}_{2})^{2} + \epsilon_{x}^{3}(\mathbf{k}_{3})^{2})Y^{3}] = Q_{x}^{2}[(3\epsilon_{x}^{1}(\mathbf{k})^{2} + 3\epsilon_{x}^{2}(\mathbf{k})^{2})Y + Y^{3}],$$
(19)

where $\epsilon_x^3(\mathbf{k})^2 + \epsilon_x^3(\mathbf{k})^2 + \epsilon_x^3(\mathbf{k})^2 = 1$, because $\epsilon^3(\mathbf{k})$ has equal components. Now, must be $3\epsilon_x^1(\mathbf{k})^2 + 3\epsilon_x^2(\mathbf{k})^2 = 2$ to obtain Equation (18). In order to prove that, it us useful to prove another statement:

$$\epsilon_x^{1^2} + \epsilon_{x,\theta}^{1^2} + \epsilon_{x,\phi}^{1^2} + \epsilon_x^{2^2} + \epsilon_{x,\theta}^{2^2} + \epsilon_{x,\phi}^{2^2} = 2,$$
 (20)

where $\epsilon_{x,\theta}^1$ is the x component of a vector obtained by rotating by an angle θ $\epsilon^1(\mathbf{k})$ around the usual direction (1,1,1), etc. It makes sense, since:

$$3\epsilon_{x}^{1^{2}} + 3\epsilon_{x}^{2^{2}} = \epsilon_{x}^{1^{2}} + \epsilon_{x,0}^{1^{2}} + \epsilon_{x,0}^{1^{2}} + \epsilon_{x}^{2^{2}} + \epsilon_{x,0}^{2^{2}} + \epsilon_{x,0}^{2^{2}} =$$

$$= \epsilon_{x}^{1^{2}} + \epsilon_{x,\frac{2\pi}{3}}^{1^{2}} + \epsilon_{x,\frac{4\pi}{3}}^{1^{2}} + \epsilon_{x}^{2^{2}} + \epsilon_{x}^{2^{2}} + \epsilon_{x,\frac{2\pi}{3}}^{2^{2}} + \epsilon_{x,\frac{4\pi}{3}}^{2^{2}} =$$

$$= \epsilon_{x}^{1^{2}} + \epsilon_{y}^{1^{2}} + \epsilon_{z}^{1^{2}} + \epsilon_{x}^{2^{2}} + \epsilon_{y}^{2^{2}} + \epsilon_{z}^{2^{2}} = 2.$$
(21)

Vectors ϵ^1 and ϵ^2 are orthogonal to each other and to ϵ^3 which lies in the (1,1,1) direction. This means that ϵ^1 and ϵ^2 lie in the same plane orthogonal to the direction (1,1,1) like their rotation at any angle. A change in coordinates

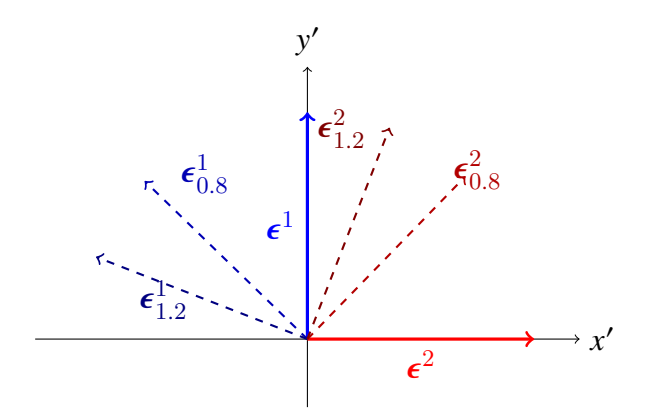


Figure 7: Unit vectors $\boldsymbol{\epsilon}^1$ on the y-axis and $\boldsymbol{\epsilon}^2$ on the x-axis, and their counterclockwise rotations by two arbitrary angles θ and ϕ (angles in radians).

leads to Figure 7, which shows ϵ^1 and ϵ^2 and two of their rotation at two random angles. With a symmetry argument, in particular, a swap of axis, the same we used before for permutations in three dimensions, we assert:

$$\epsilon_{x}^{'1^{2}} + \epsilon_{x,\theta}^{'1^{2}} + \epsilon_{x,\phi}^{'1^{2}} + \epsilon_{x}^{'2^{2}} + \epsilon_{x,\theta}^{'2^{2}} + \epsilon_{x,\phi}^{'2^{2}} = \epsilon_{y}^{'1^{2}} + \epsilon_{y,\theta}^{'1^{2}} + \epsilon_{y,\phi}^{'1^{2}} + \epsilon_{y,\theta}^{'2^{2}} + \epsilon_{y,\theta}^{'2^{2}} + \epsilon_{y,\phi}^{'2^{2}}, \quad (22)$$

which leads to:

$$2(\epsilon_{x}^{'1^{2}} + \epsilon_{x,\theta}^{'1^{2}} + \epsilon_{x,\phi}^{'1^{2}} + \epsilon_{x}^{'2^{2}} + \epsilon_{x,\theta}^{'2^{2}} + \epsilon_{x,\phi}^{'2^{2}}) =$$

$$= \epsilon_{x}^{1^{2}} + \epsilon_{x,\theta}^{'1^{2}} + \epsilon_{x,\phi}^{'1^{2}} + \epsilon_{x,\phi}^{'2^{2}} + \epsilon_{x,\phi}^{'2^{2}} + \epsilon_{y,\phi}^{'1^{2}} + \epsilon_{y,\theta}^{'1^{2}} + \epsilon_{y,\phi}^{'1^{2}} + \epsilon_{y,\phi}^{'2^{2}} + \epsilon_{y,\phi}^{'2^{2}} + \epsilon_{y,\phi}^{'2^{2}} = 6,$$

$$\Rightarrow \epsilon_{x}^{'1^{2}} + \epsilon_{x,\theta}^{'1^{2}} + \epsilon_{x,\phi}^{'1^{2}} + \epsilon_{x,\phi}^{'2^{2}} + \epsilon_{x,\theta}^{'2^{2}} + \epsilon_{x,\phi}^{'2^{2}} = 3.$$
(23)

This can be translated in three dimensions, i.e. in the previous coordinate system, obtaining:

$$\epsilon_{x}^{1^{2}} + \epsilon_{x,\theta}^{1^{2}} + \epsilon_{x}^{1^{2}} + \epsilon_{x}^{2^{2}} + \epsilon_{x,\theta}^{2^{2}} + \epsilon_{x,\phi}^{2^{2}} = \epsilon_{y}^{1^{2}} + \epsilon_{y,\theta}^{1^{2}} + \epsilon_{y,\phi}^{1^{2}} + \epsilon_{y,\phi}^{2^{2}} + \epsilon_{y,\phi}^{2^{2}} + \epsilon_{y,\phi}^{2^{2}} = \epsilon_{x,\phi}^{1^{2}} + \epsilon_{x,\phi}^{1^{2}} + \epsilon_{x,\phi}^{1^{2}} + \epsilon_{x,\phi}^{1^{2}} + \epsilon_{x,\phi}^{2^{2}} + \epsilon_{x,\phi}^{2^{2}} + \epsilon_{x,\phi}^{2^{2}} + \epsilon_{x,\phi}^{2^{2}},
3(\epsilon_{x}^{1^{2}} + \epsilon_{x,\theta}^{1^{2}} + \epsilon_{x,\phi}^{1^{2}} + \epsilon_{x}^{2^{2}} + \epsilon_{x,\phi}^{2^{2}} + \epsilon_{x,\phi}^{2^{2}} + \epsilon_{x,\phi}^{2^{2}}) = 6,
\Rightarrow \epsilon_{x}^{1^{2}} + \epsilon_{x,\theta}^{1^{2}} + \epsilon_{x,\phi}^{1^{2}} + \epsilon_{x}^{2^{2}} + \epsilon_{x,\phi}^{2^{2}} + \epsilon_{x,\phi}^{2^{2}} = 2.$$
(24)

Exactly what we need to add diagonal elements in Equation 16.

To obtain more precisely Equation (24), consider a vector \mathbf{v} on the plane orthogonal to (1, 1, 1). Rotate it by 90° around (1, 1, 1), to get $\mathbf{w} \perp \mathbf{v}$.

$$\boldsymbol{v} = \begin{pmatrix} v_x \\ v_y \\ v_z \end{pmatrix} \longrightarrow \boldsymbol{w} = \frac{1}{\sqrt{3}} \begin{pmatrix} v_z - v_y \\ v_x - v_z \\ v_y - v_x \end{pmatrix}. \tag{25}$$

Then, considering $v_x + v_y + v_z = 0$ and $w_x + w_y + w_z = 0$, we just sum the square components and obtain:

$$v_x^2 + w_x^2 = v_y^2 + w_y^2 = v_z^2 + w_z^2. (26)$$

3.1.4 Canceling cross products out

The cross products are not eliminated by merely summing a set of three rotated k vectors, but require also summing over the k vectors obtained by flipping the sign of one or more components, i.e. those reflected across the x, y, and z axes:

$$\mathbf{k}_{11} = (k_1, k_2, k_3)$$

$$\mathbf{k}_{21} = (-k_1, k_2, k_3)$$

$$\mathbf{k}_{31} = (k_1, -k_2, k_3)$$

$$\mathbf{k}_{41} = (k_1, k_2, -k_3),$$
(27)

where the first index stands for the reflection and the second stands for the permutation shown in Equation (9). In order to simplify the notation, we denote $\epsilon_{\mu}^{\lambda}(\mathbf{k}_{ij})$ by μ_{ij} , because the following proof is the same for any λ ; for example $\epsilon_{x}^{1}(\mathbf{k}_{12})$ becomes x_{12} . The matrices below show the matches between a \mathbf{k} and the cross product term related to $Q_{x}Q_{y}$ for a specific λ , Equation (8), which is not expressed because irrelevant:

$$\begin{pmatrix} \mathbf{k}_{11} & \mathbf{k}_{12} & \mathbf{k}_{13} \\ \mathbf{k}_{21} & \mathbf{k}_{22} & \mathbf{k}_{23} \\ \mathbf{k}_{31} & \mathbf{k}_{32} & \mathbf{k}_{33} \\ \mathbf{k}_{41} & \mathbf{k}_{42} & \mathbf{k}_{43} \end{pmatrix} \rightarrow \begin{pmatrix} x_{11}y_{11} & x_{12}y_{12} & x_{13}y_{13} \\ x_{21}y_{21} & x_{22}y_{22} & x_{23}y_{23} \\ x_{31}y_{31} & x_{32}y_{32} & x_{33}y_{33} \\ x_{41}y_{41} & x_{42}y_{42} & x_{43}y_{43} \end{pmatrix}. \tag{28}$$

Computing the sum $\sum_{i=1}^{3} \sum_{j=1}^{4} x_{j,i} y_{j,i}$ means summing over a single column and then sum the result for all the others. Using polarization vectors symmetries, Appendix 5:

$$x_{11} = x_{21} y_{11} = -y_{21} x_{31} = x_{41} y_{31} = -y_{41}$$

$$x_{12} = x_{32} y_{12} = -y_{32} x_{22} = x_{42} y_{22} = -y_{44} (29)$$

$$x_{13} = -x_{2.3} y_{1.3} = y_{23} x_{33} = -x_{43} y_{33} = y_{43}.$$

We show that the summation over each column vanishes:

$$x_{1i}y_{1i} + x_{2i}y_{2i} + x_{3i}y_{3i} + x_{3i}y_{3i} = 0 \quad \Rightarrow \quad \sum_{i=1}^{3} \sum_{j=1}^{4} x_{ji}y_{ji} = 0.$$
 (30)

The result is the same for every other cross product. When vectors are on one of the diagonals of the cubic first Brillouin zone, we cannot sum over all permutations and reflections because some terms are equal, so we cannot sum the same term several times. In fact, in this case it is not even necessary to sum over all permutations and reflections.

$$\mathbf{k}_{1} = (k, k, k)$$
 $\mathbf{k}_{2} = (-k, k, k)$
 $\mathbf{k}_{3} = (k, -k, k)$
 $\mathbf{k}_{4} = (k, k, -k)$,
$$(31)$$

The same argument used above leads to the canceling also of these products. The last term which has neither permutations nor reflections is $\mathbf{k} = (\pi, \pi, \pi)$. However, it is sufficient to count only his contribution to get the same simplification we get with all the other sets. This implies that every term inside the brackets in Equation (8), which multiply the cross product, vanishes and so do the last three lines of Equation (8).

$$2Q_{x}Q_{y}((\sum_{i=1}^{3}\sum_{j=1}^{4}x_{ji}y_{ji})_{1}Y_{1} + (\sum_{i=1}^{3}\sum_{j=1}^{4}x_{ji}y_{ji})_{2}Y_{2} + (\sum_{i=1}^{3}\sum_{j=1}^{4}x_{ji}y_{ji})_{3}Y_{3}) +$$

$$+2Q_{x}Q_{z}((\sum_{i=1}^{3}\sum_{j=1}^{4}x_{ji}z_{ji})_{1}Y_{1} + (\sum_{i=1}^{3}\sum_{j=1}^{4}x_{ji}z_{ji})_{2}Y_{2} + (\sum_{i=1}^{3}\sum_{j=1}^{4}x_{ji}z_{ji})_{3}Y_{3}) + (32)^{2}Y_{2} + (\sum_{i=1}^{3}\sum_{j=1}^{4}x_{ji}z_{ji})_{2}Y_{2} + (\sum_{i=1}^{3}\sum_{j=1}^{4}x_{ji}z_{ji})_{3}Y_{3}) = 0.$$

The desired form is achieved:

$$W(\mathbf{Q}) = C(T)|\mathbf{Q}|^2, \tag{33}$$

where C(T) is

$$C(T) = \frac{1}{6N} \sum_{k}^{1BZ\setminus\{0\}} \sum_{\lambda=1}^{3} \frac{\hbar}{2m\omega_{\lambda}(k)} (2n_{\lambda}(k,T) + 1).$$
 (34)

Equations (33) and (34) are the main theoretical result of the present thesis.

3.2 A Debye-like approximation

Using a Debye-like approach, we write an approximate but simpler expression for the C(T) factor:

$$\sum_{k}^{1\text{BZ}\backslash\{0\}} \sum_{\lambda=1}^{3} \to \int_{0}^{k_{D}} g(k)dk \,, \quad g(k) = \frac{3Na^{3}}{2\pi^{2}}k^{2} \,, \quad k_{D} = \frac{(6\pi^{2})^{\frac{1}{3}}}{a} \,. \tag{35}$$

Therefore:

$$C_{D}(T) = \frac{1}{6N} \int_{0}^{k_{D}} \frac{\hbar}{2mv_{s}k} \left(\frac{2}{\exp \frac{\hbar v_{s}k}{k_{B}T} - 1} + 1 \right) g(k)dk =$$

$$= \frac{1}{2N} \int_{0}^{k_{D}} \frac{\hbar}{2mv_{s}k} \left(\frac{2}{\exp \frac{\hbar v_{s}k}{k_{B}T} - 1} + 1 \right) \frac{Na^{3}}{2\pi^{2}} k^{2}dk ,$$

$$C_{D}(T) = \frac{\hbar a^{3}}{8\pi^{2}mv_{s}} \int_{0}^{k_{D}} \left(\frac{2}{\exp \frac{\hbar v_{s}k}{k_{B}T} - 1} + 1 \right) kdk . \tag{36}$$

After a change of variables, $x = \hbar v_s k/(k_B T)$, we can reformulate Eq. (36) as:

$$C_D(T) = \frac{a^3 (k_B T)^2}{8\pi^2 m \hbar v_s^2} \int_0^{\theta_D/T} \left(\frac{2}{\exp x - 1} + 1\right) x dx.$$
 (37)

By taking the low-temperature limit and using $\int_0^\infty 2x/(e^x-1)dx = \pi^2/3$, we obtain the following expression:

$$C_D(T) \simeq \frac{\hbar a^3}{16 \pi^2 m v_s} k_D^2 + (k_B T)^2 \frac{a^3}{24 m \hbar v_s^3}.$$
 (38)

On the other hand, for $T \gg \theta_D$ one can expand the exponential in Eq. (37) for small x, carry out the integration, and obtain the asymptotic high-temperature expression:

$$C_D(T) \simeq \frac{a^3 k_D}{4\pi^2 m v_s^2} k_B T \,, \tag{39}$$

where \hbar cancels out, indicating a classic (i.e. non quantum) behavior.

Based on the results illustrated above, in practice the numerical evaluation of $W(\mathbf{Q})$, can be divided into two parts. The first part consists of trivially evaluating the squared norm of \mathbf{Q} , while the second involves the computation of C(T), either based on the exact numeric method discussed above or with some approximate model formula, as discussed in the next Section.

3.3 Useful symmetries for the evaluation of C(T)

To accelerate the calculation of the summation, one can exploit the symmetry of $Y^{\lambda}(\mathbf{k})$, both under reflections and translations, allowing the summation to be performed over only a portion of the first Brillouin zone and then multiplying the result by an appropriate factor. In particular, the symmetry under reflections and permutations reduces the first Brillouin zone to the subset of points that yield independent values of Y. In practice, the symmetry with respect to reflections

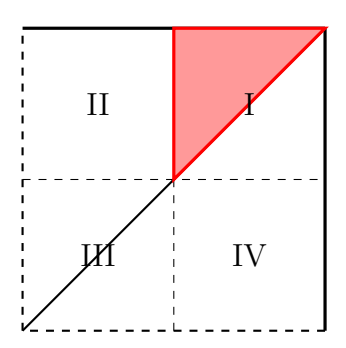


Figure 8: The square is a 2D representation of the first Brillouin zone. The top and right edges of the square are highlighted because they lie within the 1BZ. The red triangle indicates the region over which I am summing. As can be clearly seen in this simplified diagram, all points strictly inside the red triangle correspond to 7 other distinct points in the 1BZ, for a total of 8 equivalent points. In contrast, points on the diagonal and on the outer edges correspond to 3 other points, for a total of 4 equivalent points. Finally, the point at the center corresponds only to itself.

allows us to perform the **k**-points summation only over the first octant of the 1BZ. Additionally, the symmetry under rotations permits the summation to be carried out only over the piece of the first octant in which no triplet (k_1, k_2, k_3) is a permutation of another. After performing this summation, the multiplicative factor to obtain the correct value of C(T) is 8, corresponding to the reduction to the first octant, and 6, because there are 3! triplets obtainable by permuting the same three components, corresponding to the further reduction within this region, 48 in total. The main difficulty is to exclude from multiplication with 48 the boundary points inside the symmetric zone considered, in Figure 8 there is a simplified representation of what this means. The three-dimensional case is obviously more intricate, for that see Appendix B.

3.4 Size scaling for the C(T) coefficient

We are actually interested in the $N_{\text{side}} \to +\infty$ limit for the Debye-Waller factors, and thus for C(T). A direct computation of this condition is of course impossible. However, we can obtain an estimation of this quantity by a standard finite-size extrapolation, also called finite-size scaling. For a given temperature T, we plot the C(T) as a function of the inverse of N_{side} . This illustrates the size scaling, and allows us to extract the desired infinite-size value. Figure 9 reports the finite-size

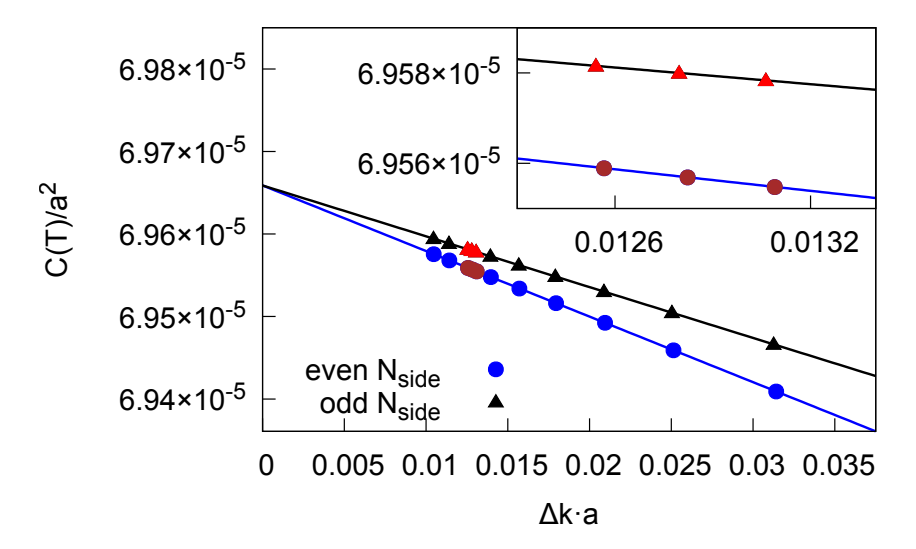


Figure 9: Size scaling of C(T) as a function of $\Delta k \propto N_{\rm side}^{-1}$, at temperature T=1 θ_D . Black and blue points: numerically computed values of C(T). Lines: linear fits based uniquely on the 3 highlighted (red or brown) points. The two scalings (even/odd $N_{\rm side}$ appear approximately linear. This makes it possible to use a simple linear regression to extract the limiting C(T) value for $\Delta k \to 0$ with good accuracy. As can be seen the two different linear regressions lead to very similar intercepts at $\Delta k = 0$. Eventually we take the average between those two intercepts as our best estimate for the thermodynamic limit of C(T). Inset: detail of the points used for the linear fits.

scaling of C(T) as a function of $\Delta k \propto N_{\rm side}^{-1}$: it clearly shows an approximately linear scaling of C(T). First, we need to explain why Fig. 9 shows two separate trends instead of just one.

Figure 10 sketches a one-dimensional explanation of the observed even-odd effect. Recall that every addendum in the summation in Eq. (34) contributes proportionally to $\omega_{\lambda}(\mathbf{k})^{-1}$, and that $\omega_{\lambda}(\mathbf{k}) \propto |\mathbf{k}|$ for small $|\mathbf{k}|$, see the acoustic behavior of the phonon dispersion reported in Fig. 2. As a result, the \mathbf{k} closest to the origin give the greatest contribution. Now consider two first Brillouin (1BZ) zone grids: one built using odd N_{side} and one using even N_{side} , e.g. the successive integer. In the even case the origin must be excluded from the summation, while in the odd case the grid involves no \mathbf{k} at the origin. Consider the region around the origin of for these two 1BZ grids, containing a similar number of \mathbf{k} points, in such a way that we can establish a one-to-one correspondence between two \mathbf{k}

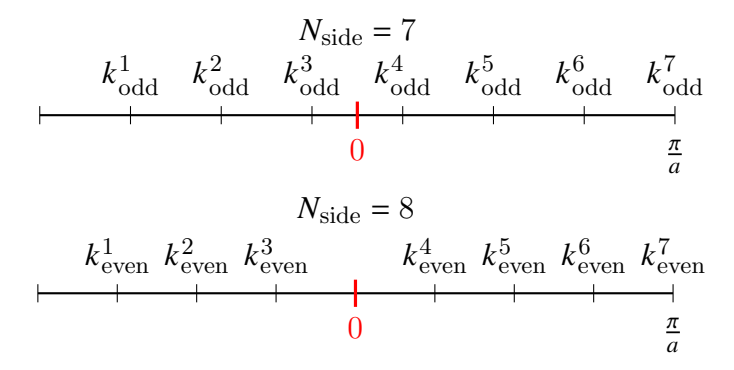


Figure 10: Two sampling grids for a one dimensional 1BZ, with $N_{\rm side} = 7$ (top) and $N_{\rm side} = 8$ (bottom). Observe that the k points closest to the origin for the odd $N_{\rm side} = 7$ grid are closer to the origin than the closest ones of the $N_{\rm side} = 8$ grid. The tics enumeration shows a one-to-one correspondence between the points within the two 1BZ with different $N_{\rm side}$ based on the closeness to the origin.

points around the origin. The pair of shortest k points in the odd grid always sit closer to the origin than the corresponding pair in the even grid. The formula for the uniform 1BZ grid for the $N_{\rm side} \times N_{\rm side} \times N_{\rm side}$ simple-cubic lattice is the following:

$$\mathbf{k} = 2\pi(n_x, n_y, n_z), \quad n_\alpha = -\frac{1}{2} + \frac{1}{N_{\text{side}}}, -\frac{1}{2} + \frac{2}{N_{\text{side}}}, \dots, \frac{1}{2}.$$
 (40)

If, for example, N_{side} is even, then the shortest k vector is:

$$|\boldsymbol{k}_{\text{odd}}^{i}| = |2\pi(\frac{1}{2(N_{\text{side}} - 1)}, 0, 0)| = \frac{\pi}{N_{\text{side}} - 1} < \frac{2\pi}{N_{\text{side}}} = |2\pi(\frac{1}{N_{\text{side}}}, 0, 0)| = |\boldsymbol{k}_{\text{even}}^{i}|$$

$$\Rightarrow \omega_{\lambda}(\boldsymbol{k}_{\text{odd}}^{i}) < \omega_{\lambda}(\boldsymbol{k}_{\text{even}}^{i}) \Rightarrow \omega_{\lambda}(\boldsymbol{k}_{\text{odd}}^{i})^{-1} > \omega_{\lambda}(\boldsymbol{k}_{\text{even}}^{i})^{-1},$$

$$(41)$$

where the index i stands for the one-to-one correspondence sketched in Fig. 10. This shows that the addends from the odd- N_{side} grid give a larger, dominant contribution near the origin: this is the term responsible for the even/odd splitting in the C(T) scaling shown in Fig. 9.

Eventually, as illustrated in Fig. 9, to evaluate the infinite-size estimation of C(T) we carry out two separate linear fits of the numeric finite-size estimations obtained by evaluating Eq. (34) with the following $N_{\rm side}$ values: (481, 491, 501) and (480, 490, 500). We then take the average between the two intercepts of those

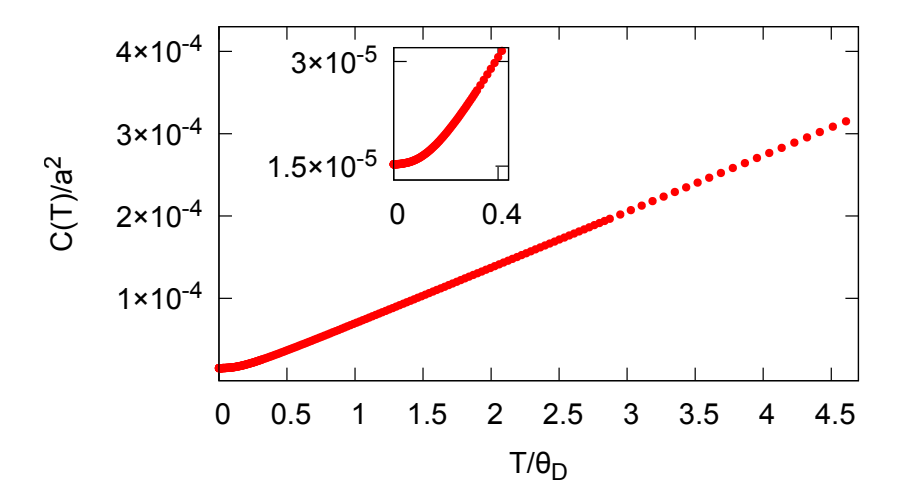


Figure 11: Temperature dependence of C(T). The reported values reflect the infinite-size limit, obtained by linear extrapolation plus averaging of the intercepts as discussed in the text. Inset: detail of the low-temperature region. This result applies to the simple-cubic lattice, with the mechanical parameters K, K' = K/2, m, and a listed in Table 1.

two fits (which are extremely close anyway, a deviation $\leq 0.0002\%$) as our best estimate for the $N_{size} \to \infty$ limit of C(T).

4 Results

With the recipe to evaluate the infinite-size limit of C(T) detailed in the previous Section, we report the resulting overall dependence in Fig. 11. C(T) grows approximately linearly at temperatures exceeding the Debye temperature. At lower temperature, C(T) rounds off quadratically to a constant as the Debye approximation predicts, Eq. (38). The order of magnitude of $C(T)/a^2$, in the 10^{-4} range, reflects the numerical value of Planck's constant $\hbar = 1.09 \times 10^{-4} \, a^2 (Km)^{1/2}$ in model units, for the parameters assumed in Table 1.

Figure 12 shows a comparison of the numerically exact C(T), Eq. (34) with the approximate one obtained through the Debye model, Eq. (37): significant differences are visible. These discrepancies are caused by an overall overestimation of the vibrational frequencies that the Debye model does, see Fig. 13.

The deviations of the Debye model from the exact C(T) can be corrected by

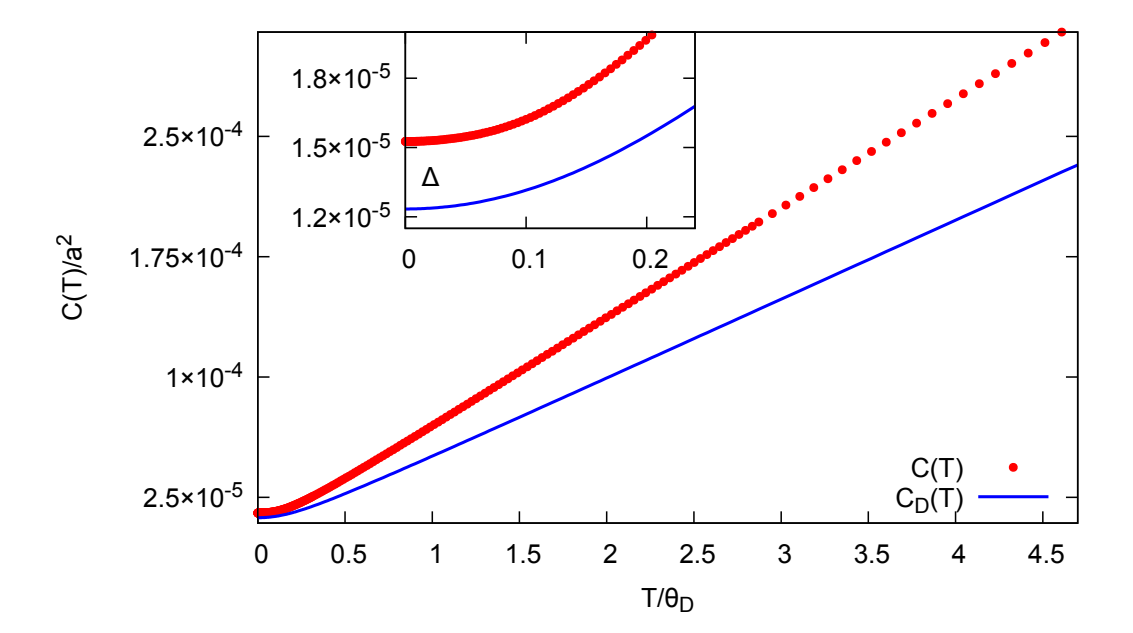


Figure 12: A comparison between the numerically exact C(T) of Fig. 11 and Eq. (34) – blue dots, and the approximate Debye form $C_D(T)$, Eq. (37) – red line, where speed of sound has been tuned to match exactly the $C(T) \propto T^2$ raise at small T. The Debye model underestimates the exact result by approximately $2.922 \times 10^{-6} \, a^2$ at T=0; this underestimation increases with temperature, and at large $T \gg \theta_D$, it deviates approximately linearly with temperature. Inset: detail of the discrepancy at low temperatures. Δ stands for the difference $C(0) - C_D(0)$.

(i) introducing an additive term Δ that brings the T=0 value to the exact one:

$$\Delta = C(0) - C_D(0) \simeq 2.922 \times 10^{-6} \ a^2, \tag{42}$$

where $C_D(0)$ is provided by Eq. (38). Additionally, we add the contribution of two "Einstein"-type oscillators, as follows:

$$C_{\text{fit}}(T) = C_D(T) + \Delta + \frac{p_1}{\exp\frac{p_2}{T} - 1} + \frac{p_3}{\exp\frac{p_4}{T} - 1}.$$
 (43)

By carrying out a least-square fit of 224 numerically determined values of C(T) between T = 0 θ_D and T = 5 θ_D , we obtain $p_1 \simeq (-3.406 \times 10^{-6} \pm 1.22 \times 10^{-7})$ a^2 , $p_2 \simeq (2328 \pm 20.97)$ Ka^2/k_B , $p_3 \simeq (9.227 \times 10^{-6} \pm 1.30 \times 10^{-7})$ a^2 and $p_4 \simeq (828.9 \pm 1.51)$ Ka^2/k_B Figure 14 reports the result of this fit.

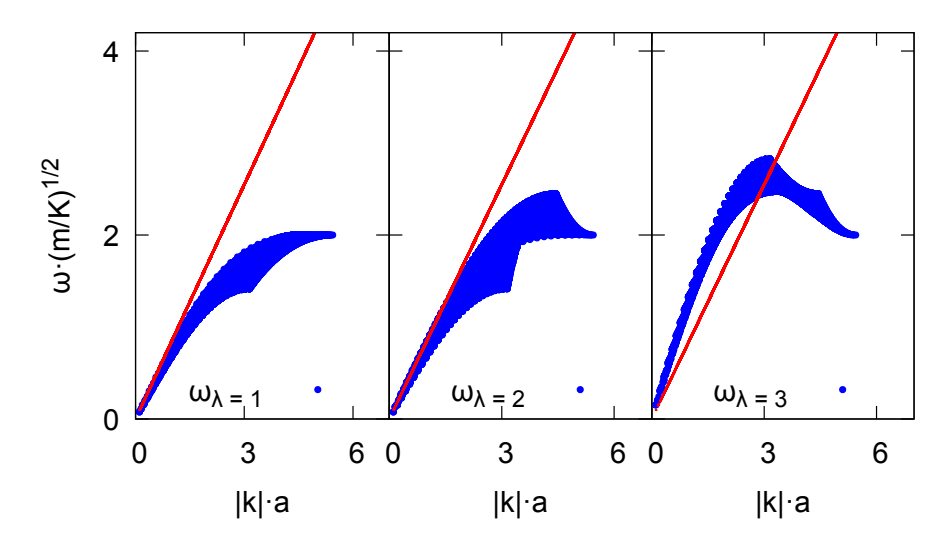


Figure 13: A comparison between the Debye phonon dispersion and the exact frequencies reported separately for the 3 phonon branches $\lambda=1,2,3$. The broad band of blue points results from the vibrational frequencies being calculated along numerous directions in \mathbf{k} space, each associated with its peculiar acoustic dispersion. For the transverse branches $\lambda=1,2,$ the Debye model systematically overestimates the exact frequency across the majority of the 1BZ. The longitudinal branch $\lambda=3$ has a range of $|\mathbf{k}|$ where the exact frequency is larger than the Debye model, but for large $|\mathbf{k}|$ near the 1BZ edge, even the longitudinal phonon comes below the Debye dispersion. On average, we can safely state that the Debye approximation overestimates the vibrational frequencies.

Figure 15 reports the Debye-Waller factor $\exp(-W(\mathbf{Q}))$ over an extremely broad \mathbf{Q} range, far larger than the one employed for the friction computation [1], which extends out to $Q_{\text{max}} \simeq 72.5 \ a^{-1}$. For temperatures lower than θ_D , in the $0-Q_{\text{max}}$ range the attenuation is smaller than 10%, therefore we expect a small difference between the friction evaluated without and with the Debye-Waller factor. Even at T=0 a nonzero attenuation persists, due to the zero-point motion effect, but, as shown in Fig. 15, this correction is quite small in the relevant \mathbf{Q} -region. In the previous work [1], the integration domain $\mathbf{\Omega}$ for the integration implied by the calculation of phonon friction, Eq. (1), was restricted to a finite box, thanks to the rapid decay of the Fourier transform $\tilde{V}(|\mathbf{Q}|)$ of the interaction potential. However, different interaction potentials may lead to different large- $|\mathbf{Q}|$ behavior of $\tilde{V}(|\mathbf{Q}|)$, possibly requiring a larger integration domain. As illustrated

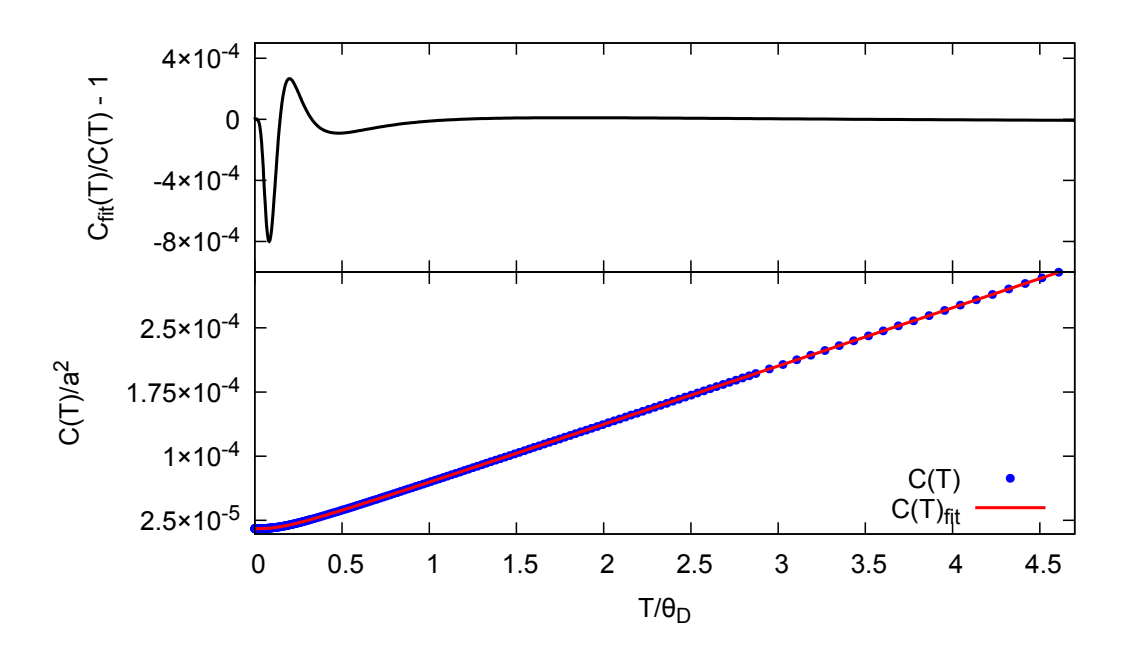


Figure 14: The best-fit C_{fit} , Eq. (43); top panel: its relative deviation from the numerically exact C(T).

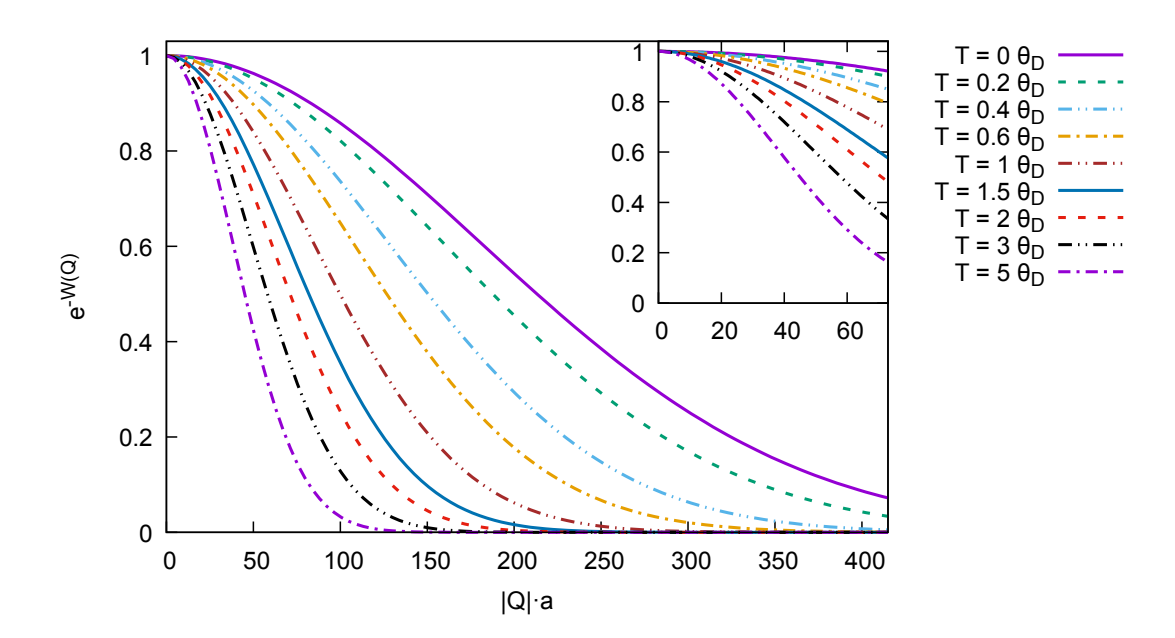


Figure 15: The Debye-Waller factor $e^{-W(Q)}$ as a function of the length of the wave vector Q. The higher is temperature the stronger is attenuation effect. The effect becomes relevant for high magnitudes of Q. Inset: the Q range is restricted to the size of integration domain used for the friction evaluation.

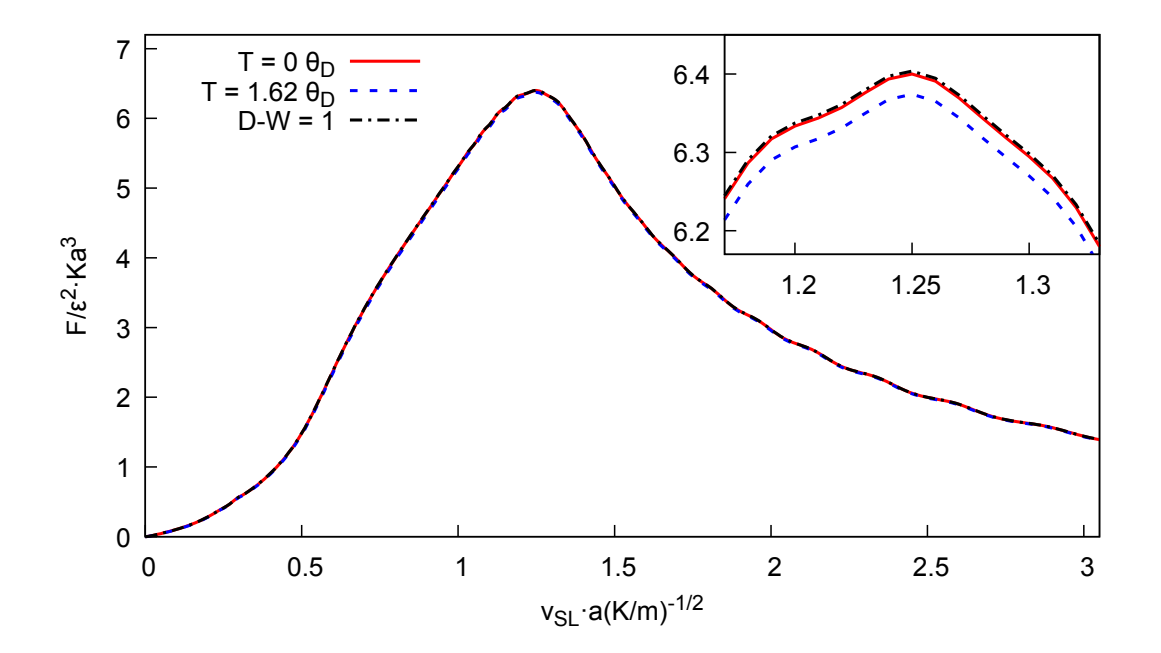


Figure 16: Comparison of the phonon friction evaluated (i) with the Debye-Waller factors approximated with unity (dot-dashed line); (ii) with the Debye-Waller factors appropriate for T=0 (solid line); and (iii) with the Debye-Waller factors for an intermediate temperature $T=1.62~\theta_D$ (dashed line). The **Q**-integrations are carried out over a mesh of 400^3 points, and the slider-crystal interaction potential $V(r) = \epsilon \left[\left(\frac{\sigma^2 + d^2}{r^2 + d^2} \right)^6 - 2 \left(\frac{\sigma^2 + d^2}{r^2 + d^2} \right)^3 \right]$. As expected, accounting for a Debye-Waller factor smaller than unity primarily leads to a decrease in friction, best visible at the peak (inset).

in Fig. 15, inclusion of the exact Debye-Waller factor, improves the integral convergence, especially at large temperature. This allows one to use this method to investigate a wider range of interactions.

Figures 16 and 17 report the comparison between the phonon friction evaluated without Debye-Waller factors [1], with one that includes those factors, as evaluated in the present thesis, for T=0 and for an intermediate temperature $T=1.62\,\theta_D$. The direct comparison indicates that replacing the Debye-Waller factors with unity is not such a bad approximation. Especially when zooming on the peak, small deviations are visible, and those deviations could only increase at higher temperature.

Instructed by Fig. 17, we try to fabricate an approximate rule to quickly evaluate friction at any temperature. We start by defining the following dimen-

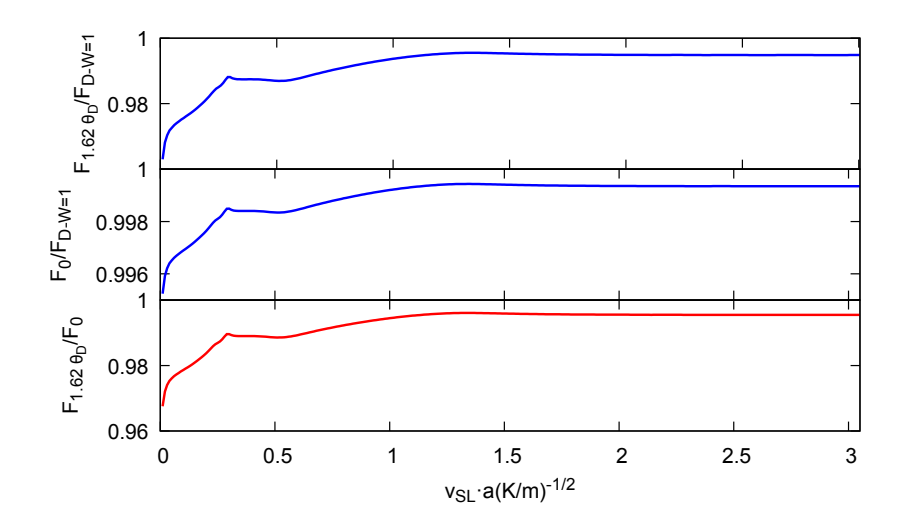


Figure 17: Quotient of friction evaluated for two different temperatures or approximating the Debye-Waller factor with unity. The velocity dependence of these ratios are quite similar, strongly hinting at the possibility of a simplified law to evaluate friction at any temperature based on the friction evaluation carried out without Debye-Waller factors.

sionless friction ratio:

$$\frac{F_0(v_{\rm SL})}{F_{\rm D-W=1}(v_{\rm SL})} \equiv r(v_{\rm SL}) \quad \Rightarrow \quad \frac{F_T(v_{\rm SL})}{F_{\rm D-W=1}(v_{\rm SL})} \simeq r^{-b(T)}(v_{\rm SL}) \,, \tag{44}$$

where b(T) is an increasing function of T.

Equation (44) leads to Fig. 18. There is a way to determine b(T), using the fact that C(T) is small. For $\max(|\mathbf{Q}|, |\mathbf{Q} + \mathbf{G}|) \ll C(T)^{-1}$, we perform an expansion of the Debye-Waller factor:

$$e^{-W(\mathbf{Q})-W(\mathbf{Q}+\mathbf{G}_{\perp})} = e^{-(|\mathbf{Q}|^{2}+|\mathbf{Q}+\mathbf{G}_{\perp}|^{2})C(T)} \simeq 1 - (|\mathbf{Q}|^{2}+|\mathbf{Q}+\mathbf{G}_{\perp}|^{2})C(T), \qquad (45)$$

$$\Rightarrow F_{T}(v_{SL}) \simeq \dots \left[1 - (|\mathbf{Q}|^{2}+|\mathbf{Q}+\mathbf{G}_{\perp}|^{2})C(T)\right] \dots = F_{\text{no DW}}(v_{SL}) - P(v_{SL})C(T). \qquad (46)$$

Here $P(v_{SL})$ is obtained from Eq. (1) by substituting the Debye-Waller factor with $|\mathbf{Q}|^2 + |\mathbf{Q} + \mathbf{G}_{\perp}|^2$ assuming that the relavant integration converges. If we substitute Eq. (46) into Eq. (44), omitting the v_{SL} dependence, we obtain:

$$\frac{F_T(v_{\rm SL})}{F_{\rm DW=1}(v_{\rm SL})} \simeq \frac{F_{\rm DW=1}(v_{\rm SL}) - P(v_{\rm SL})C(T)}{F_{\rm DW=1}(v_{\rm SL})} = 1 - \frac{P(v_{\rm SL})C(T)}{F_{\rm DW=1}(v_{\rm SL})} \simeq \exp\left(-\frac{P(v_{\rm SL})C(T)}{F_{\rm DW=1}(v_{\rm SL})}\right) \,. \tag{47}$$

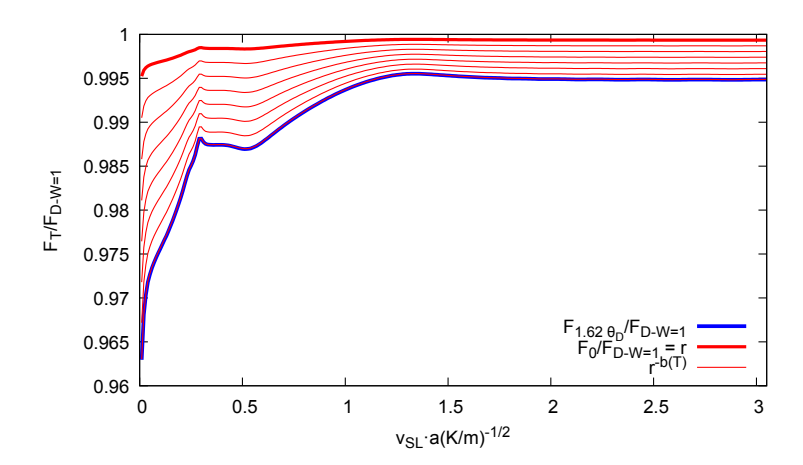


Figure 18: The ratio $r = F_0/F_{\text{D-W=1}}$ (red solid line). For another temperature, e.g. $T = 1.62\theta_D$, then we can obtain $F_T/F_{\text{D-W=1}}$ as $r^{-b(T)}$. Thin lines: $r^{-b(T)}$ for increasing b(T), until at the right value $b(T) \simeq 7.89$ there is a perfect match with $F_{1.62\theta_D}/F_{\text{D-W=1}}$.

Observe further that

$$\frac{F_0(v_{\rm SL})}{F_{\rm DW=1}(v_{\rm SL})} = \exp\left(-\frac{P(v_{\rm SL})C(0)}{F_{\rm DW=1}(v_{\rm SL})}\right) = r(v_{\rm SL}) \quad \Rightarrow \quad b(T) = \frac{C(T)}{C(0)}. \tag{48}$$

By comparing the expression for b(T) with the formula for C(T), Eq. (34), we formulate an interpretation of b(T) as an effective boson factor $(2n_{\lambda}(\mathbf{k}) + 1)$, namely, the weighted average of the boson factor over the 1BZ, and over the three phonon branches. Indeed, notice that the temperature dependence of $(2n_{\lambda}(\mathbf{k}) + 1)$, Fig. 3, is similar overall to that of C(T), Fig. 11.

5 Discussion and Conclusion

We prove a factorization of the Debye-Waller exponent into a temperature-dependent factor C(T), and a \mathbf{Q} -dependent term, namely $|\mathbf{Q}|^2$. We focus on C(T) and derive its exact expression, and a Debye-type approximation thereof. We take advantage of the obtained explicit formula to compute the phonon friction, at a specific temperature, with a computational cost similar to that of previous work [1] where the Debye-Waller factors were approximated with unity.

Moreover, we obtain a nicely well approximate method to evaluate phonon friction at any temperature using a relatively simple formula, based on the numerical evaluation of friction done with the Debye-Waller factors replaced by unity.

Finally, we observe that the rapid large-|Q| decay of the Debye-Waller factor could be taken advantage of to investigate slow-decaying Fourier-transformed slider-crystal interactions.

A A few basic crystal symmetries

We obtain phonon polarization vectors $\boldsymbol{\epsilon}_{\lambda}(\boldsymbol{k})$ and frequencies $\omega_{\lambda}(\boldsymbol{k})$ by diagonalizing the dynamical matrix $D_{\mu\nu}$. For these monoatomic crystals, the eigenvalue equation:

$$\omega_{\lambda}^{2}(\mathbf{k})\,\epsilon_{\lambda\mu}(\mathbf{k}) = \sum_{\nu} D_{\mu\nu}(\mathbf{k})\,\epsilon_{\lambda\nu}(\mathbf{k}) \tag{49}$$

where the elements of the dynamical matrix are:

$$D_{xx}(\mathbf{k}) = \frac{2K}{m} (1 - \cos(k_x a)) + \frac{2K'}{m} (2 - \cos(k_x a)\cos(k_y a) - \cos(k_x a)\cos(k_z a)),$$

$$D_{yy}(\mathbf{k}) = \frac{2K}{m} (1 - \cos(k_y a)) + \frac{2K'}{m} (2 - \cos(k_x a)\cos(k_y a) - \cos(k_y a)\cos(k_z a)),$$

$$D_{zz}(\mathbf{k}) = \frac{2K}{m} (1 - \cos(k_z a)) + \frac{2K'}{m} (2 - \cos(k_x a)\cos(k_z a) - \cos(k_y a)\cos(k_z a)),$$

$$D_{\mu\nu}(\mathbf{k}) = \frac{2K'}{m}\sin(k_\mu a)\sin(k_\nu a).$$
(50)

From here, it is possible to deduce a symmetry by reflection with respect to the origin, because the minus sign inside the elements of the dynamical matrix does not affect the cosines and the sines multiply each other, so as to cancel the minus sing out:

$$\omega_{\lambda}(-\mathbf{k}) = \omega_{\lambda}(\mathbf{k})$$

$$\epsilon_{\lambda}(-\mathbf{k}) = \epsilon_{\lambda}(\mathbf{k}).$$
(51)

It is also possible to derive the symmetry under single component reflection: $k_{\mu} \rightarrow -k_{\mu}$, indicating k' the vector obtained with such a transformation. The symmetries are the following:

$$\omega_{\lambda}(\mathbf{k}') = \omega_{\lambda}(\mathbf{k}),$$

$$\epsilon_{\lambda,\mu}(\mathbf{k}') = \epsilon_{\lambda,\mu}(\mathbf{k}), \quad \epsilon_{\lambda,\nu}(\mathbf{k}') = -\epsilon_{\lambda,\nu}(\mathbf{k}), \quad \text{for } \nu \neq \mu.$$
(52)

See [1].

B Symmetry for faster C(T) computation

Here is a more specific calculation to exploit the $Y_{\lambda}(\mathbf{k})$ symmetry, or equally $\omega_{\lambda}(\mathbf{k})$ symmetry. Referring to Table 2, one can compute C(T) faster in the following way:

$$C(T) = \frac{1}{6N} \sum_{n=1}^{14} I_n \sum_{k \in S_n} \sum_{\lambda} Y_{\lambda}(k).$$
 (53)

n	$S_n \equiv \text{Set of } \mathbf{k}$	$I_n \equiv \text{Symmetry factor}$
1	$0 < x < y < z < \pi$	$8 \cdot 6 = 48$
2	$0 = x < y < z < \pi$	$4 \cdot 6 = 24$
3	$0 < x = y < z < \pi$	$8 \cdot 3 = 24$
4	$0 < x < y = z < \pi$	$8 \cdot 3 = 24$
5	$0 < x < y < z = \pi$	$4 \cdot 6 = 24$
6	$0 = x = y < z < \pi$	$2 \cdot 3 = 6$
7	$0 < x = y = z < \pi$	$8 \cdot 1 = 8$
8	$0 < x < y = z = \pi$	$2 \cdot 3 = 6$
9	$0 = x < y = z < \pi$	$4 \cdot 6 = 12$
10	$0 = x < y < z = \pi$	$2 \cdot 6 = 12$
11	$0 < x = y < z = \pi$	$4 \cdot 3 = 12$
12	$0 = x = y < z = \pi$	$1 \cdot 3 = 3$
13	$0 < x = y = z = \pi$	$1 \cdot 1 = 1$
14	$0 = x < y = z = \pi$	$1 \cdot 3 = 3$
15	$0 = x = y = z < \pi$	$1 \cdot 1 = 1$

Table 2: The first columns is just an enumeration done for clearness. The second contains all the set one needs to distinguish to avoid summing over terms that are repeated or that do not exist inside the first Brillouin zone, where x, y, z indicate the components of k. The third column contains the symmetry factor to multiply to the summation over the set on the left to get the entire first Brillouin zone. The explicit multiplication used to obtain the symmetry factor is intentional: the first factor represents the number of reflections that can be applied to a term within the set to yield a point inside the first Brillouin zone; the second factor represents the number of permutations that can be performed for the same purpose. For completeness, the point (0,0,0), i.e. set 15, is listed here, but in the computation of C(T) has to be excluded.

References

[1] G. Riva, G. Piscia, N. Trojani, G.E. Santoro, E. Tosatti, and N. Manini, Phys. Rev. B 112, 054310 (2025).